Available online at www.sciencedirect.com
ScienceDirect
Chinese Journal of Aeronautics 23(2010) 537-548
Chinese Journal of Aeronautics
www.elsevier.com/locate/cja

Numerical Simulation of Dynamic Response of Fiber Reinforced Ceramic Matrix Composite Beam with Matrix Cracks Using Multiscale Modeling

Gao Xiguang, Song Yingdong*, Sun Zhigang, Hu Xuteng

College of Energy and Power Engineering, Nanjing University of Aeronautics and Astronautics, Nanjing 210016, China

Received 26 November 2009; accepted 10 April 2010

Abstract

A multiscale method for simulating the dynamic response of ceramic matrix composite (CMC) with matrix cracks is developed. At the global level, the finite element method is employed to simulate the dynamic response of a CMC beam. While at the local level, the multiscale mechanical method is used to estimate the stress/strain response of the material. A distributed computing system is developed to speed up the simulation. The simulation of dynamic response of a Nicalon/CAS-II beam being subjected to harmonic loading is performed as a numerical example. The results show that both the stress/strain responses under tension and compressive loading are nonlinear. These conditions result in a different response compared with that of elastic beam, such as: 1) the displacement response is not symmetric about the axis of time; 2) in the condition of small external load, the response at first order natural frequency is limited within a finite range; 3) decreasing the matrix crack space will increase the displacement response of the beam.

Keywords: ceramic matrix composite; dynamic analysis; vibration analysis; multiscale analysis; matrix crack; interface debonding

1. Introduction

Comparing with monolithic ceramic, ceramic matrix composite (CMC) exhibits a remarkable increase in strain-to-failure due to the multiple energy dissipation mechanism. Much works have been done to estimate the static performance of CMC[1-5]. This kind of material is often used to manufacture the parts of aeroengine, rocket, and so on due to the high temperature resistant capability. In these systems the dynamic problem cannot be ignored since the external dynamic force may be the main driver of failure. Thus, the dynamic problems of CMC structure are getting more and more attention in recent years. Both experimental researches[6-11] and theoretical analyses[12-15] have been widely performed in this field.

J. Lankford[6] investigated the high-strain-rate compressive failure mechanisms of fiber reinforced CMC. The results were compared with those of composite damage development at low strain rates and the dynamic failure of monolithic ceramics. They found that the fiber direction affected the dynamic compressive strength of CMC greatly. P. T. Jaminet, et al.[7] used the piezoelectric ultrasonic composite oscillator technique (PUCOT) to measure the damping and dynamic elastic moduli of certain kinds of ceramics and CMC at elevated temperatures. C. Wang, et al.[8] investigated the damping behavior of C/C composites which were fabricated by chemical vapor infiltration (CVI) method, in the low-frequency range by means of a pendulum method. The results implied that the internal friction of the C/C composites decreased with the decrease of the volume fraction of fibers. Meanwhile, the internal friction of the composites was found to increase with increase of porosity. Q. Zhang, et al.[9] measured the internal friction of 2D C/SiC composites fabricated by CVI method through the dynamical mechanical analysis (DMA) method at different frequencies from room temperature to 400 ℃ in the atmosphere. The results showed that the damping peak of the composites increased gradually and the temperature of the peak shifted to the lower temperature with the increase of PyC interphase thickness. Q. Zhang, et al.[10] used the DMA method to measure the damping properties of C/SiC composites at different frequencies from room

*Corresponding author. Tel.: +86-25-84895778.
E-mail address: ydsong@nuaa.edu.cn
Foundation items: Jiangsu Postdoctoral Science Foundation (0902013C); Innovation Foundation for Young Teachers in University of Aeronautics and Astronautics (Y1024-054)

doi: 10.1016/S1000-9361(09)60252-1

temperature to 400 ºC in the atmosphere. The results showed that SiC coating and heat treatment decreased the damping capacity of C/SiC composites and the damping peak disappeared or decreased within the testing temperature range. M. Liu, et al.[11] investigated the compressive properties of 2D C/SiC composites by quasi-static experiments and split-Hopkinson pressure bar system. The results showed that the dynamic compressive stress-strain curves were nonlinear. Based on the experimental results, they proposed a new constitutive model which was fit for one dimensional dynamic compressure.

In the area of theoretical investigation, C. Cho, et al.[12] developed a method to estimate the interfacial shear in ceramic composites from frictional heating measurements. They first assumed a forward slip zone and a reversed slip zone at the interface and then derived the formulas for the work of interface slip by using shear-lag method. Even though the original goal of the work was not directly related to the damping capacity of CMC, the results were used by other researchers to estimate the energy dissipation due to interface friction. V. Birman, et al.[13] employed the energy dissipation formula developed by C. Cho, et al.[12] to estimate the damping in unidirectional composites with matrix cracks, cross-ply laminates with tunneling cracks in transverse layers, and bridging cracks in longitudinal layer. V. Birman, et al.[14] extended the theory to angle-ply laminate and investigated the effects of the frequency and magnitude of local dynamic stresses on the loss factor. Based on the theory of Y. M. Han, et al.[16], V. Birman, et al.[15] developed an approach to the analysis of cross-ply composite beams with distributed damage and distributed stiffness subjected to static bending. They also investigated the effect of matrix crack on the stiffness and natural frequency. The results showed that the changes of stiffness and natural frequency of CMC beam due to matrix crack were small.

Based on the above literature review, it can be seen clearly that up to now the experimental studies of CMC dynamic problem are focused on the dynamic failure mechanism, testing damping capacity, testing dynamic elastic modulus, and dynamic constitutive behavior; while the theoretical researches are restricted to the estimation of damping capacity and natural frequency. However, little work has been done to simulate the dynamic response of CMC structure.

Previous researches have evidenced that the property of CMC is commonly affected by the external load[17]. For example, the stiffness of CMC laminates may be changed under repeating loading due to open (under tension) and closed (under compression) cracks. Thus, it is inappropriate to model the dynamic response by the linear dynamic governing equations. This will greatly increase the difficulty of modeling the dynamic response of CMC, but this kind of modeling is important for conducting structure design.

The dynamic relation between the stress and strain of CMC is quite complicated. According to the above literature review, people have not yet understood all the mechanisms of CMC dynamic constitutive relation clearly. V. Birman, et al.[13-14] considered that the matrix crack, interface friction and the elastic moduli of fiber and matrix were the main factors which affected the dynamic response of CMC structure. Based on the classical shear-lag model, they developed a micromechanics method to predict damping capacity of CMC. However, their method could not be used to model the dynamic stress/strain response under complicated loading history, and the Poisson's effect and the nonlinear interface contact were not taken into account.

In this article, in order to simulate the nonlinear dynamic response of CMC structure, a multiscale modeling method which includes global and local analyses is developed. At the local level, a unit-cell model is used to estimate the stress/strain response of CMC; while at the global level, the response of CMC beam is simulated by finite element method (FEM). The dynamic constitutive model is developed from homocentric column model which considers the Poisson's effect and the nonlinear interface contact. Following the theoretical analysis, as a numerical example, the stress/strain response of Nicalon/CAS-II material is predicted and compared with the experimental data. The dynamic response of CMC beam subjected to harmonic load is also simulated. The difference between the responses of CMC and elastic beam is also discussed. Recent works about the multiscale modeling of composite can be seen from Refs.[18]-[21]. However, it should be noted that an analytical prediction of dynamic response of CMC structure with damage has not been thoroughly investigated.

2. CMC Damage Mechanisms

Comparing with the polymer matrix composite, the damping coefficients of ceramic fiber and matrix are quite small[22-24]. The energy dissipation of CMC increases dramatically with the increasing matrix cracks. That means the damping capability of CMC is affected by the damage greatly. So, it is necessary to understand the damage pattern of CMC.

In the case of a unidirectional CMC material being subjected to axial tensile load, an extensive amount of damage will develop within the material. Matrix crack, interface slip and debonding, fiber failure and fiber pull-out are the main damage mechanisms during under tensile loading. In the process of preparing CMC, lots of small defects may be introduced into the material. When loading the material, matrix cracks will be initiated from these small defects and then will be propagated in the planes perpendicular to the fibers. When the matrix cracks approach the fiber, an alternative damage pattern may happen depending on the strength of fiber/matrix interface. In most cases, the interface is weak and the matrix crack will propagate around the fiber and induce interface debonding. As the load is continually increasing, the number of matrix cracks increases and then reaches a saturation state. Thus, a larger percentage of the load will be carry by the fibers

due to the degradation of matrix. Eventually, if fibers are broken, the fiber may be pulled out from the matrix. When the number of broken fibers achieves a critical value, the laminate will be failed[25-26].

In the case of small external load, such as the small amplitude vibration, the number of broken fibers is so small that the effect of broken fibers can be ignored. Thus, it is appropriate to consider the effects of matrix crack and interface slip only. In addition, since the external load is small, the space between adjacent matrix cracks and the debonding length of fiber/matrix interface are assumed to be constants during loading.

3. Simulating Dynamic Response of CMC

3.1. Unit-cell model of CMC

Based on the damage mechanisms described previously, a simplified unit-cell model is used to predict the stress-strain response of the unidirectional fiber reinforced CMC. First, we assumed that the arrangement of the fibers in matrix is uniform and symmetric. In particular, the fibers are assumed to be prismatic and continuous and embedded in the matrix with the form of regular rectangular array (see Fig.1). In addition to this assumption, the constituents of fiber and matrix are assumed to be intact. Therefore, the fiber and matrix are responding in perfectly linear-elastic modes.

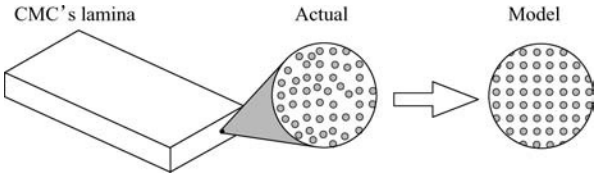

Fig.1 Assumed geometric arrangement of fibers.

Once a matrix crack appears, it will spread to the entire cross section of lamina soon. Thus, every crack is considered as an infinitely thin plane being perpendicular to the loading axis. Experimental data indicate that the space between two adjacent matrix cracks is approximately uniform[27-28]. In addition to the matrix cracks, the interface debonding also occurs during loading. Since the stress concentration at the tip of matrix crack, the interface debonding is assumed to be originated from the crack planes, spreaded uniformly around the fibers, and of constant length for all fiber/crack pairs.

The above-mentioned assumptions allow the composite to be modeled by a simple unit-cell model consisting of a single fiber and surrounding matrix. The length of the cell is equal to the average crack space which is denoted by L. Interface debonding is symmetric about the plane of matrix crack which is perpendicular to the fiber and we use d to denote the length of interface debonding at each side (see Fig.2, where R is the radius of unit cell).

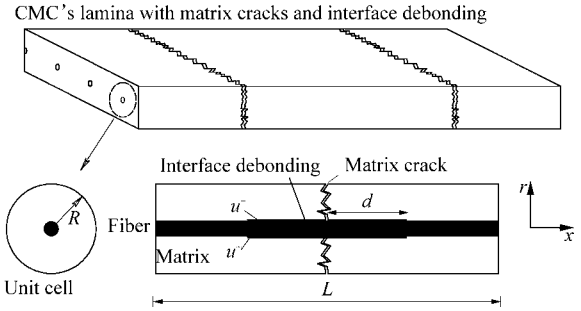

Fig.2 Illustration of unit cell with matrix cracks and interface debonding.

In the debonding area, the interface shearing stress τ_i is governed by the Coulomb's friction law as follows

$$\left.\begin{aligned} &\tau_i = \tau_{\max} && \tau_i \geq \tau_{\max} = \mu\sigma_r \\ &u_x^+ = u_x^-, u_r^+ = u_r^- && \tau_i < \tau_{\max} = \mu\sigma_r \end{aligned}\right\} \quad (1)$$

where μ is the coefficient of friction, σ_r the radial stress at the interface, and u^+ and u^- are the interface displacements of fiber and matrix respectively (see Fig.2).

CMC is often prepared at a high temperature of 1 000 °C. During process of cooling down to room temperature, an initial compressive stress is induced at the contacting area of fiber and matrix due to their different thermal expansion coefficients. The difference of radial displacements between fiber and matrix can be estimated by

$$\Delta u_r = u_{r\mathrm{m}} - u_{r\mathrm{f}} = r_\mathrm{f}(\alpha_\mathrm{m} - \alpha_\mathrm{f})\left|\Delta T\right| \quad (2)$$

where $u_{r\mathrm{m}}$ and $u_{r\mathrm{f}}$ are the radial displacements of matrix and fiber, α_m and α_f the thermal expansion coefficients of matrix and fiber respectively, ΔT is the difference between CMC preparing temperature and room temperature, and r_f the radius of fiber.

FEM is employed to model the stress/strain response of CMC. The unit cell is discretized by a four-node axisymmetric element which is shown in Fig.3. In addition to showing the layout of the fiber and matrix elements, Fig.3 also shows the boundary conditions of axial loading. Since the unit cell is distributing periodically in material, the uniform displacement boundary condition is employed at each side of unit cell, as follows:

$$\left.\begin{aligned} &u_x\big|_{x=0} = u_r\big|_{r=0} = 0 \\ &u_x\big|_{x=L} = \bar{\varepsilon}_x L \end{aligned}\right\} \quad (3)$$

where $\bar{\varepsilon}_x$ denotes the global strain in the axial direction.

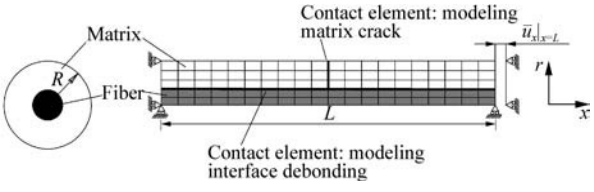

Fig.3 Finite element model of unit cell for modeling stress/strain response of CMC with matrix crack and interface debonding.

Since all the loads are transmitted through the cross section at the end of unit cell, the global axial stress is defined as the average of the axial stress of this plane, as follows:

$$\bar{\sigma}_x = \frac{2\int_0^R \sigma_x(x=0) r \mathrm{d}r}{R^2} \tag{4}$$

The friction in debonding zone is modeled by the contact and friction element which obeys the law of friction expressed by Eq.(1). When the unit cell is being compressed, the matrix crack at the center of unit cell may be closed and then transmit the loads. Therefore, the contact element should also be employed at the surface of matrix crack. The initial compressive stress between fiber and matrix is modeled by setting the initial offset displacement of contact element in debonding region. The initial offset displacement Δu_r is expressed by Eq.(2).

The process of modeling the strain/stress response is given as follows. First, a global strain is given, and then the displacement at the end of unit cell is calculated by Eq.(3) and applied to the finite element model. Through performing the finite element analysis, the stress field of the unit cell is estimated. By using Eq.(4), we obtain the global stress corresponding to the given global strain. Repeating the above-mentioned process, we can obtain all the global stress for a complicated loading history (the load is in the form of global strain). Thus, a numerical constitutive model of the CMC is constructed and expressed by

$$\bar{\sigma}_x = \bar{\sigma}_x(\bar{\varepsilon}_x) \tag{5}$$

Since the calculation of nth step depends on the calculated result of (n–1)th step, a small load increment is necessary for a complicated loading history.

3.2. Finite elment simulation of nonlinear vibration of CMC beam

(1) Governing equations

As an example, the problem of a laminated cantilever CMC beam of unit width subjected to an axial stress $\hat{\sigma}(t)$ which is applied on the free end is considered. The CMC beam is assumed to be homogeneous at the global level and the constitutive equation is given by Eq.(5). Thus, the equation of longitudinal vibration of the beam at the global level can be written as

$$\frac{\partial \bar{\sigma}_x}{\partial x} = \rho \frac{\partial^2 u}{\partial t^2} \tag{6}$$

where ρ is the mass density of beam. The solution of Eq.(6) must satisfy the dynamic boundary conditions:

$$\left.\begin{aligned} u(x=0) &= 0 \\ \bar{\sigma}_x\big|_{x=l} &= \hat{\sigma}(t) \end{aligned}\right\} \tag{7}$$

where l denotes the length of the beam.

In the case of linear-elastic beam, Eq.(6) can be expressed as

$$E\frac{\partial^2 u}{\partial x^2} = \rho \frac{\partial^2 u}{\partial t^2} \tag{8}$$

where E is the elastic modulus of the beam. Eq.(8) can be solved by assuming the u has the following form:

$$u = U(x)T(t) \tag{9}$$

where $U(x)$ and $T(t)$ are the functions of coordinate x and time t respectively. In the case of CMC beam, it's difficult to solve Eq.(6) analytically since the nonlinear behavior of CMC. Thus, we employ Galerkin method to obtain the approximate solution of Eq.(6). Firstly, the equivalent integral form of Eqs.(6)-(7) is expressed as

$$\int_0^l \delta u\left(\frac{\partial \bar{\sigma}_x}{\partial x} - \rho\frac{\partial^2 u}{\partial t^2}\right)\mathrm{d}x - \delta u(\bar{\sigma}_x - \hat{\sigma}(t))\big|_{x=l} = 0 \tag{10}$$

Performing the integration by parts and simplification, the expression of $\int_0^l \delta u(\partial \bar{\sigma}_x/\partial x)\mathrm{d}x$ can be rewritten as

$$\int_0^l \delta u\frac{\partial \bar{\sigma}_x}{\partial x}\mathrm{d}x = \delta u\bar{\sigma}_x\big|_{x=l} - \int_0^l \delta u_{,x}\bar{\sigma}_x \mathrm{d}x \tag{11}$$

Substituting Eq.(11) into Eq.(10) gives the following formulation:

$$\rho\int_0^l \delta u\frac{\partial^2 u}{\partial t^2}\mathrm{d}x + \int_0^l \delta u_{,x}\bar{\sigma}_x\mathrm{d}x = \delta u\hat{\sigma}(t)\big|_{x=l} \tag{12}$$

We employ the two-node linear element to discretize the beam as shown in Fig.4. Then, displacement within ith element can be expressed as

$$u = \frac{u_i}{l_i}(x_{i+1} - x) + \frac{u_{i+1}}{l_i}(x - x_i) \tag{13}$$

where u_i and x_i denote the displacement and the coordinate of ith node respectively, and l_i is the length of ith element.

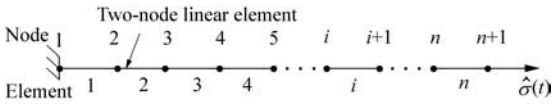

Fig.4 Finite element model of CMC beam.

Based on Eq.(13), the strain and acceleration of a point in ith element can be expressed as

$$\bar{\varepsilon}_x^i = \frac{\partial u}{\partial x} = \frac{u_{i+1}}{l_i} - \frac{u_i}{l_i} \tag{14}$$

$$\ddot{u} = \frac{\ddot{u}_i}{l_i}(x_{i+1} - x) + \frac{\ddot{u}_{i+1}}{l_i}(x - x_i) \tag{15}$$

where $\ddot{u}_i$ denotes the acceleration of ith node. Substituting Eqs.(13)-(15) into Eq.(12) gives the discretized form of Eq.(12) as follows:

$$\rho\sum_i\int_{L_i}\left[\frac{\delta u_i}{l_i}(x_{i+1}-x)+\frac{\delta u_{i+1}}{l_i}(x-x_i)\right]\cdot\left[\frac{\ddot{u}_i}{l_i}(x_{i+1}-x)+\frac{\ddot{u}_{i+1}}{l_i}(x-x_i)\right]\mathrm{d}x+\sum_i\int_{L_i}\left(\frac{\delta u_{i+1}}{l_i}-\frac{\delta u_i}{l_i}\right)\bar{\sigma}_x(x)\mathrm{d}x=\delta u_{n+1}\hat{\sigma}(t)\big|_{x=l} \quad (16)$$

Simplifying Eq.(16) gives that

$$\sum_i\left[\delta u_i(\ddot{u}_iM_{i1}+\ddot{u}_{i+1}M_{i3})+\delta u_{i+1}(\ddot{u}_iM_{i2}+\ddot{u}_{i+1}M_{i4})\right]+\sum_i\left[\delta u_{i+1}\int_{L_i}\frac{\bar{\sigma}_x}{l_i}\mathrm{d}x-\delta u_i\int_{L_i}\frac{\bar{\sigma}_x}{l_i}\mathrm{d}x\right]=\delta u_{n+1}\hat{\sigma}(t)\big|_{x=l} \quad (17)$$

where

$$\left.\begin{aligned}M_{i1}&=\int_{L_i}\rho\frac{(x_{i+1}-x)^2}{l_i^2}\mathrm{d}x=\frac{\rho l_i}{3}\\M_{i2}=M_{i3}&=\int_{L_i}\rho\frac{(x_{i+1}-x)(x-x_i)}{l_i^2}\mathrm{d}x=\frac{\rho l_i}{6}\\M_{i4}&=\int_{L_i}\rho\frac{(x-x_i)^2}{l_i^2}\mathrm{d}x=\frac{\rho l_i}{3}\end{aligned}\right\} \quad (18)$$

Since Node 1 is constrained, u_1 and δu_1 are equal to zero constantly. Thus, we obtain a linear system of n algebraic equations containing n unknowns u_2, u_3, $\cdots$, u_{n+1}. It can be written as

$$\left.\begin{aligned}&\ddot{u}_iM_{i1}+\ddot{u}_{i+1}M_{i3}+\ddot{u}_{i-1}M_{(i-1)2}+\ddot{u}_iM_{(i-1)4}=\\&\int_{L_i}\frac{\bar{\sigma}_x}{l_i}\mathrm{d}x-\int_{L_{i-1}}\frac{\bar{\sigma}_x}{l_{i-1}}\mathrm{d}x\quad(i=2,3,\cdots,n)\\&\ddot{u}_nM_{n2}+\ddot{u}_{n+1}M_{n4}=\hat{\sigma}(t)\big|_{x=l}-\int_{L_n}\frac{\bar{\sigma}_x}{l_n}\mathrm{d}x\end{aligned}\right\} \quad (19)$$

Transforming Eq.(19) into matrix form, we can obtain

$$\boldsymbol{M}\ddot{\boldsymbol{u}}=\boldsymbol{F} \quad (20)$$

where the mass matrix $\boldsymbol{M}$, acceleration vector $\ddot{\boldsymbol{u}}$ and load vector $\boldsymbol{F}$ are given by

$$\boldsymbol{M}=\begin{bmatrix}M_{21}+M_{14}&M_{22}&\cdots&0\\M_{23}&M_{31}+M_{24}&\cdots&0\\0&M_{23}&\cdots&0\\0&0&\cdots&0\\\vdots&\vdots&&\vdots\\0&0&\cdots&M_{n2}\\0&0&\cdots&M_{n4}\end{bmatrix}^{\mathrm{T}} \quad (21a)$$

$$\ddot{\boldsymbol{u}}=[\ddot{u}_2\quad\ddot{u}_3\quad\cdots\quad\ddot{u}_{n+1}]^{\mathrm{T}} \quad (21b)$$

$$\boldsymbol{F}=\begin{bmatrix}\int_{L_2}(\bar{\sigma}_x/l_2)\mathrm{d}x-\int_{L_1}(\bar{\sigma}_x/l_1)\mathrm{d}x\\\int_{L_3}(\bar{\sigma}_x/l_3)\mathrm{d}x-\int_{L_2}(\bar{\sigma}_x/l_2)\mathrm{d}x\\\vdots\\\hat{\sigma}(t)\big|_{x=l}-\int_{L_n}(\bar{\sigma}_x/l_n)\mathrm{d}x\end{bmatrix} \quad (21c)$$

Since the nonlinear behavior of CMC, it is difficult to solve Eq.(20) with the method of mode superposition. Thus, we employ the direct integration methods involving the central difference method and the Newmark method to obtain the solution of each time step.

(2) Central difference method

Within the theoretical framework of central difference method, the acceleration is expressed as[29]

$$\ddot{\boldsymbol{u}}_t=\frac{1}{\Delta t^2}(\boldsymbol{u}_{t-\Delta t}-2\boldsymbol{u}_t+\boldsymbol{u}_{t+\Delta t}) \quad (22)$$

The displacement solution for time $t+\Delta t$ is obtained by using Eq.(20) for time t, i.e.

$$\boldsymbol{M}\ddot{\boldsymbol{u}}_t=\boldsymbol{F}_t \quad (23)$$

Substituting the expression of $\ddot{\boldsymbol{u}}_t$ written as Eq.(22) into Eq.(23), we obtain

$$\frac{\boldsymbol{M}}{\Delta t^2}\boldsymbol{u}_{t+\Delta t}=\boldsymbol{F}_t+\frac{2\boldsymbol{M}}{\Delta t^2}\boldsymbol{u}_t-\frac{\boldsymbol{M}}{\Delta t^2}\boldsymbol{u}_{t-\Delta t} \quad (24)$$

From which, we can find $\boldsymbol{u}_{t+\Delta t}$. It should be noted that using the central difference method, the calculation of $\boldsymbol{u}_{t+\Delta t}$ involves $\boldsymbol{u}_t$ and $\boldsymbol{u}_{t-\Delta t}$. Therefore, to calculate the solution at time Δt, a special starting procedure must be used. Since $\boldsymbol{u}_0$, $\dot{\boldsymbol{u}}_0$ and $\bar{\sigma}_x$ are known, $\boldsymbol{F}_t$ can be calculated using Eq.(21). Eq.(23) can be used to obtain $\ddot{\boldsymbol{u}}_0$. Therefore, the displacement vector at time $-\Delta t$ can be calculated by

$$\boldsymbol{u}_{-\Delta t}=\boldsymbol{u}_0-\Delta t\dot{\boldsymbol{u}}_0+\frac{\Delta t^2}{2}\ddot{\boldsymbol{u}}_0 \quad (25)$$

Table 1 summarizes the calculation flow of conducting the integration with the computer.

Table 1 Step-by-step solution using central difference method

1) Initial calculation:
(a) Initialize $\boldsymbol{u}_0$, $\dot{\boldsymbol{u}}_0$, and $\bar{\sigma}_x$.
(b) Form mass matrix $\boldsymbol{M}$ and load vector $\boldsymbol{F}$ by Eq.(21).
(c) Select time step Δt, and calculate $\boldsymbol{u}_{-\Delta t}$ by Eq.(25).
(d) Calculate $\boldsymbol{u}_{\Delta t}$ by Eq.(24).
2) For each time step:
(a) Calculate $\boldsymbol{u}_{t+\Delta t}$ by Eq.(24).
(b) Calculate global strain $\bar{\varepsilon}^i_{x(t+\Delta t)}$ of each element by Eq.(14).
(c) Calculate global stress $\bar{\sigma}^i_{x(t+\Delta t)}$ of each element by Eq.(5).
(d) Calculate load vector $\boldsymbol{F}_{t+\Delta t}$ by Eq.(21).
(e) Let $\boldsymbol{u}_{t-\Delta t}=\boldsymbol{u}_t$, $\boldsymbol{u}_t=\boldsymbol{u}_{t+\Delta t}$, and $\boldsymbol{F}_t=\boldsymbol{F}_{t+\Delta t}$, then go back to Step (a).

(3) Newmark method

The Newmark integration method can also be understood to be an extension of the linear acceleration method[29]. The following assumptions are used:

$$\dot{\boldsymbol{u}}_{t+\Delta t} = \dot{\boldsymbol{u}}_t + [(1-\delta)\ddot{\boldsymbol{u}}_t + \delta\ddot{\boldsymbol{u}}_{t+\Delta t}]\Delta t \tag{26}$$

$$\boldsymbol{u}_{t+\Delta t} = \boldsymbol{u}_t + \dot{\boldsymbol{u}}_t\Delta t + \left[\left(\frac{1}{2}-\alpha\right)\ddot{\boldsymbol{u}}_t + \alpha\ddot{\boldsymbol{u}}_{t+\Delta t}\right]\Delta t^2 \tag{27}$$

where α and δ are parameters determined by the required integration accuracy and stability. If these parameters satisfy the following conditions:

$$\left.\begin{aligned}&\delta \geq 0.5\\ &\alpha \geq 0.25(0.5+\delta)^2\end{aligned}\right\} \tag{28}$$

The Newmark method will be of unconditional stability[29].

The displacement solution for time $t + \Delta t$ is obtained by using Eq.(20) for time $t + \Delta t$, i.e.

$$\boldsymbol{M}\ddot{\boldsymbol{u}}_{t+\Delta t} = \boldsymbol{F}_{t+\Delta t} \tag{29}$$

Through Eq.(27), the equation of $\ddot{\boldsymbol{u}}_{t+\Delta t}$ expressed with $\boldsymbol{u}_{t+\Delta t}$ can be obtained, and then substituting the obtained equation into Eq.(29), we obtain the expression of $\boldsymbol{u}_{t+\Delta t}$ as follows:

$$\frac{1}{\alpha\Delta t^2}\boldsymbol{M}\boldsymbol{u}_{t+\Delta t} = \boldsymbol{F}_{t+\Delta t} + \boldsymbol{M}\left[\frac{1}{\alpha\Delta t^2}\boldsymbol{u}_t + \frac{1}{\alpha\Delta t}\dot{\boldsymbol{u}}_t + \left(\frac{1}{2\alpha}-1\right)\ddot{\boldsymbol{u}}_t\right] \tag{30}$$

Based on Eq.(5), Eq.(15) and Eq.(21), the load vector $\boldsymbol{F}_{t+\Delta t}$ can be expressed as the function of $\boldsymbol{u}_{t+\Delta t}$, i.e. $\boldsymbol{F}_{t+\Delta t}(\boldsymbol{u}_{t+\Delta t})$. Thus, Eq.(30) is a nonlinear equation set of n algebraic equations containing the unknown displacement $\boldsymbol{u}_{t+\Delta t}$ only. It can be solved by numerical method such as Newton method. The complete algorithm using the Newmark integration method is given in Table 2.

Table 2 Step-by-step solution using Newmark integration method

1) Initial calculation:
(a) Initialize $\boldsymbol{u}_0$, $\dot{\boldsymbol{u}}_0$ and $\bar{\sigma}_x$.
(b) Form mass matrix $\boldsymbol{M}$ and load vector $\boldsymbol{F}$ by Eq.(21).
(c) Select time step Δt and parameters α and δ which satisfy Eq.(28).
(d) Calculate $\boldsymbol{u}_{\Delta t}$ by Eq.(30).
2) For each time step:
(a) Calculate $\boldsymbol{u}_{t+\Delta t}$ by Eq.(30).
(b) Calculate global strain $\bar{\varepsilon}^i_{x(t+\Delta t)}$ of each element by Eq.(14).
(c) Calculate global stress $\bar{\sigma}^i_{x(t+\Delta t)}$ of each element by Eq.(5).
(d) Calculate load vector $\boldsymbol{F}_{t+\Delta t}$ by Eq.(21).
(e) Let $\boldsymbol{u}_{t-\Delta t} = \boldsymbol{u}_t$, $\boldsymbol{u}_t = \boldsymbol{u}_{t+\Delta t}$, and $\boldsymbol{F}_t = \boldsymbol{F}_{t+\Delta t}$, then go back to Step (a).

3.3. Distributed computing scheme

Based on the theory presented above, the simulating process includes two levels of computation. In the global level, the dynamic response of beam is simulated by the central difference method or Newmark method. In the local level, the stress/strain response is estimated by the unit cell model of CMC. This two levels computing scheme will be time-consuming if the number of nodes is increased to a large number. In order to speed up the process, a distributed computing system is designed as shown in Fig.5.

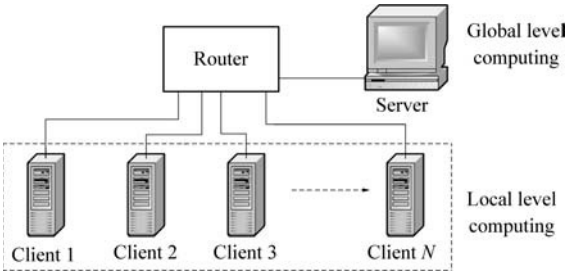

Fig.5 Distributed computing system for multiscale simulating of dynamic response of CMC beam.

The system is composed of a server and several clients. The server performs global computing and sends the global strains of nodes to the clients. Each client receives the global strain of one or more nodes and performs the local computing. Then the client sends the results back to the server. At last, the server gives the global strain for next time step.

Since the most time of entire process is taken by the local analysis, the distributed computation scheme can speed up the computing greatly. For example, considering a simulation including 10 nodes and 8 000 time steps, if each local analysis takes one second, the entire process take 80 000 seconds which is about 22.2 hours. If 10 clients are used, all local analyses for a time step will be performed at the same time. Thus, only one second will be used for a time step, and the entire process will take only 2.22 hours.

4. Results and Discussion

In order to prove the capability of the method developed above, a numerical example for Nicalon/CAS-II material is presented. Both the stress/strain response under repeating loading and the dynamic displacement response subjected to harmonic loading are predicted.

4.1. Estimating stress/strain response of CMC

Calculation is performed for a typical Nicalon/CAS-II material with the following properties[12]: the elastic modului of fiber and matrix are E_f=200 GPa and E_m=88 GPa, the volume fraction of fiber is v_f=0.35, r_f=7.3 μm, α_f=3.1×10^{-6} /°C, α_m=4.5×10^{-6} /°C, and the temperature difference between the experimental proc-

ess and processing process is $\Delta T = -1\,000$ °C. To achieve the constant matrix crack space, the specimen is first pre-fatigued for 100 000 cycles within a fixed stress range of 10-180 MPa. After approximately 100 000 cycles, the mean crack space approached a plateau at approximately 198 μm[12].

Fig.6 shows the mesh of the unit cell model. A 2D four-node axisymmetric element is used. The symmetry axis is x axis. We denote the fiber/matrix interface and the contact region of matrix cracks by black lines in Fig.6. The offset displacement between fiber and matrix is calculated by Eq.(2). The length of the unit cell model is equal to the mean crack space, i.e. 198 μm. The gray region stands for the fiber and the white region denotes the matrix. Based on the radius and volume fraction of fiber, the radius of unit cell can be calculated by following equation:

$$R = r_{\mathrm{f}} \Big/ \sqrt{v_{\mathrm{f}}} \tag{31}$$

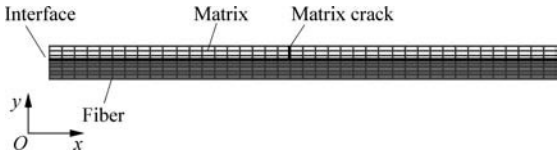

Fig.6 Finite element model of unit cell used for predicting stress/strain behavior of Nicalon/CAS-II.

Using the data given above, the stress/strain behavior is modeled by the unit cell model developed previously. Fig.7 shows the predicted results being compared with the experimental data which are taken from Ref.[12] and has a stable hysteresis loop. It can be seen that with the value of 0.025 for the interfacial frication coefficient μ the predicted result is in good agreement with the experimental stress/strain data. The value of μ seems reasonable given that the fiber/matrix bond in this type of composite is extremely weak since the degradation of interface after pre-fatigue.

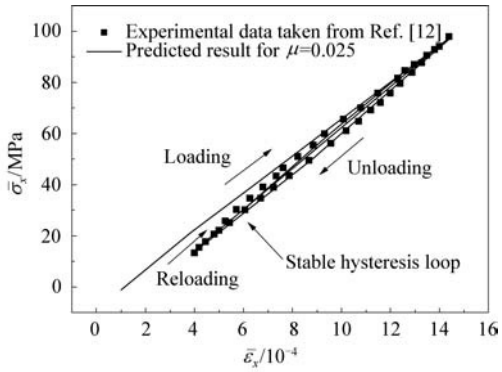

Fig.7 Comparison of predicting stress/strain response with experimental data of Nicalon/CAS-II material.

The stress/strain response of this material subjected to loading history including compressive loading is illustrated in Fig.8 (where E_{c} is the compressive modulus). The loading history involves a tensile loading up to $\bar{\varepsilon}_x = 0.001\,442\,9$, an unloading down to $\bar{\varepsilon}_x = 0$, a compressive loading up to $\bar{\varepsilon}_x = -0.001$ and a final unloading down to $\bar{\varepsilon}_x = 0$. The result shows that the stress/strain response of being subjected to compressive loading appears to be nonlinear. This can be explained by deformation at local level which is illustrated in Fig.9. When the global stress is reduced to zero, the fiber near the matrix crack is slipped into the matrix. The axial load borne by the fiber is transmitted to the matrix through the interface shear stress caused by slipping. Fig.10 shows the axial stress distributions of fiber and matrix when the global strain is approximately equal to 0.000 25. In this case, the stress field within the material is self-balanced, so the global stress is close to zero. On the other hand, in the view of microstructure, the fiber is pulled out by matrix while the matrix is compressed by fiber. Therefore, a part of the fiber is still left outside the plane of matrix crack and causes the residual strain (Fig.9(a)).

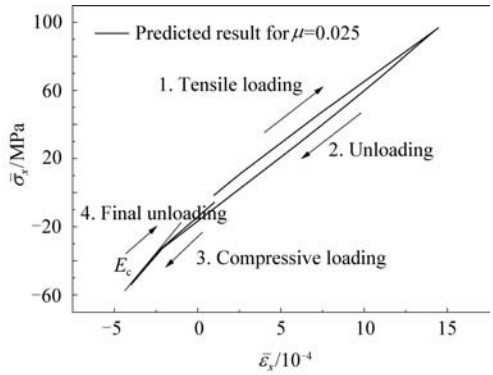

Fig.8 Stress/strain response of Nicalon/CAS-II material under tension and compressive loading.

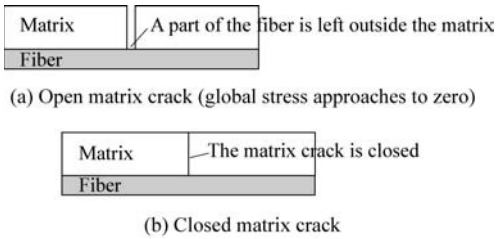

Fig.9 Microstructure of CMC in cases of open and closed matrix cracks.

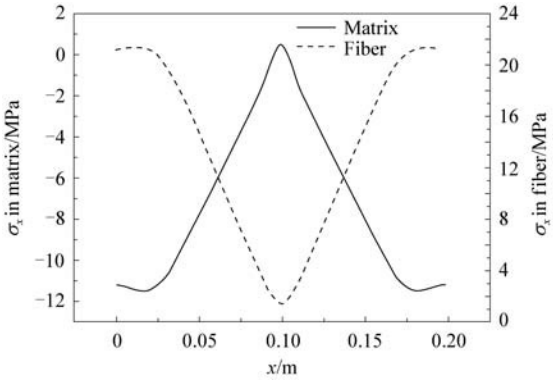

Fig.10 Stress distributions in unit cell when global stress close to zero.

When the material is being subjected to compressive loading, the fiber will be pressed into the matrix first. Due to the frictional slip, the stress/strain response is still nonlinear until the matrix crack is closed. When the fiber is completely pressed into the matrix, both sides of the matrix crack will be in contact with each other (see Fig.9(b)), and then the material will be appeared to be linear as illustrated in Fig.8. At this moment, the elastic modulus of material is close to the modulus of intact material. In this article, E_c in Fig.8 is about 126 GPa which is close to 122 GPa for the elastic modulus of the intact material reported by Ref.[12].

4.2. Simulating dynamic response of CMC beam

The dynamic response of CMC beam is simulated here by the FEM presented in Section 3.2. The length of beam is equal to 0.2 m and the mass density is equal to 2.578 5×10^3 kg/m^3. Firstly, the response of the beam which is subjected to axial periodic stress (i.e. $\hat{\sigma}(t)=\sigma_0\sin(2\pi ft)$) being applied on the free end is simulated by Newmark method. The amplitude and the frequency of the external load are 100 MPa and 100 Hz respectively. The displacement response of point $x=l$ during the first 15 cycles is presented in Fig.11(a). The result is compared with the response of an elastic beam which is illustrated in Fig.11(b). The length and mass density of the elastic beam are 0.2 m and 2.578 5×10^3 kg/m^3 respectively. The elastic modulus of the elastic beam is 80 GPa which is equal to the average elastic modulus of Nicalon/CAS-II.

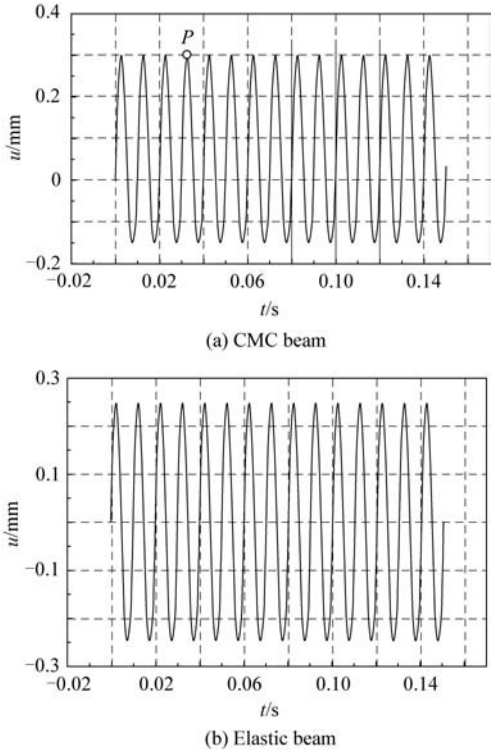

Fig.11 Comparing dynamic responses of CMC and elastic beams (frequency of external load is 100 Hz).

The result shows that both the displacement responses of CMC and elastic beams are periodic response. The frequency of the response is equal to 100 Hz. However, due to the nonlinear character of CMC beam, the response is not symmetric about the axis of u=0.

Fig.12 presents the displacement responses of the CMC and elastic beams at 3 000 Hz which are simulated by central difference method. Since the effect of the wave propagation in the beams, the displacement responses are not strictly periodic. However the time internal of the first twelve wave peaks is about 3.663×10^{-3} s, so the average period is 3.333×10^{-4} s which is close to the period of external load.

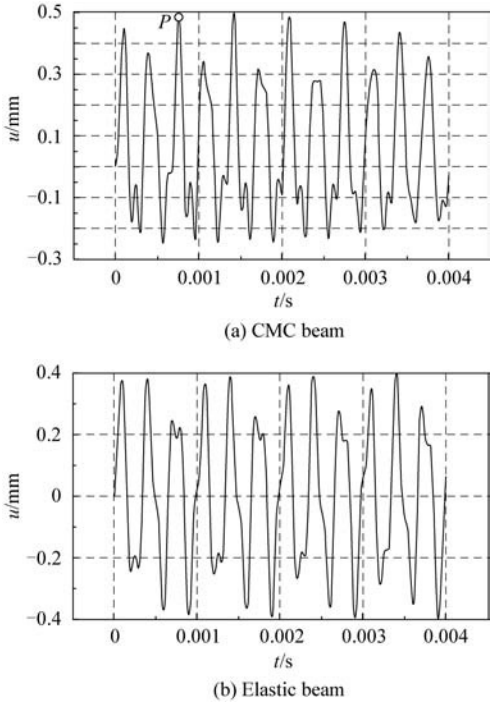

Fig.12 Comparing dynamic responses of CMC and elastic beams (frequency of external load is 3 000 Hz).

The natural frequency of the elastic beam is given by the following equation

$$\left.\begin{aligned} f_i &= \frac{(2i-1)a}{4l} \quad (i=1,2,\cdots) \\ a &= \sqrt{\frac{E}{\rho}} \end{aligned}\right\} \tag{32}$$

Substituting the average elastic modulus, the mass density and the length of the beam into Eq.(32) (i.e. E=80 GPa, ρ=2.578 5×10^3 kg/m^3, l=0.2 m) gives the first order natural frequency of the CMC beam, that is f_1=6 963 Hz. Fig.13 illustrates the displacement response of the CMC and elastic beams at 7 000 Hz which is close to f_1. We can see that the amplitude of the beams is quite greater than the responses at other frequencies. However, the response of the elastic beam is divergent while the displacement of the CMC beam is restrained within a limited range. This result implies

that the damping caused by the interface friction decreases the resonance of the beam.

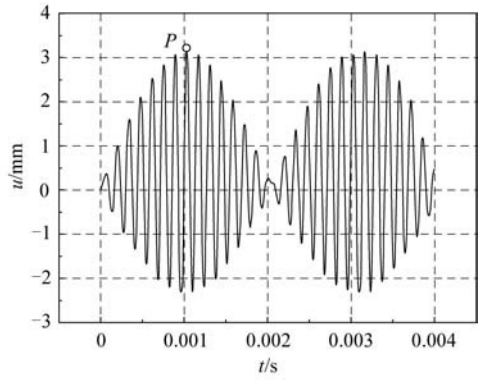

(a) CMC beam

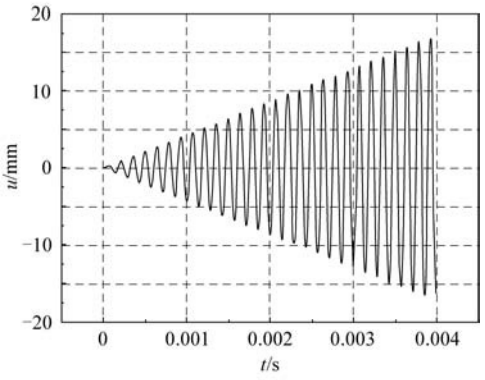

(b) Elastic beam

Fig.13 Comparing dynamic responses of CMC and elastic beams (frequency of external load is 7 000 Hz).

In order to study the dynamic response of the entire beam, we record the displacement of each node at the moment denoted by "*P*" in Figs.11-13, and then obtain the nondimensional displacement distribution presented in Fig.14.

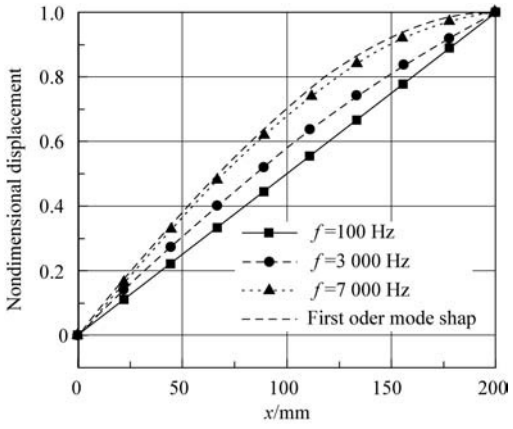

Fig.14 Nondimensional distributions along CMC beam.

The result shows that the displacement distribution of the beam is almost a straight line when the frequency of external load is quite low. However, the displacement distribution approaches to the first order modal of the elastic beam when the frequency of external load is close to the first order natural frequency.

4.3. Convergence and stability of algorithm

As mentioned in Section 3.2, the Newmark method will be unconditional stable, while the central difference method is conditional stable. The time step length Δt of central difference method should satisfy the following condition to make the algorithm stable[29]:

$$\left.\begin{aligned} \Delta t \le \Delta t_{\mathrm{cr}} = L_{\mathrm{min,ele}} / C \\ C = \left(E/\rho\right)^{1/2} \end{aligned}\right\} \tag{33}$$

where Δt_{cr} is the critical time step length, $L_{\mathrm{min,ele}}$ the length of the minimum element, and E and ρ are the elastic modulus and mass density of material respectively.

However, the elastic modulus of CMC depends on the level of external load as illustrated in Figs.7-8. In the case of unidirectional Nicalon fiber reinforced CAS-II composite, the average elastic modulus is about 80 GPa if it is subjected to tension load. The elastic modulus will increase to about 122 GPa, if the material is subjected to compress load. The critical time step lengths for these two cases are $3.989\,6\times10^{-6}$ s and $3.230\,7\times10^{-6}$ s respectively. Thus the time step length for central difference method should be shorter than $3.230\,7\times10^{-6}$ s to make the algorithm be stable.

In addition to the stability requirement, the algorithm should be convergent too. Theoretically, if the time step length is small enough, both the central difference method and the Newmark method should converge to the accurate solution. However, the time step length cannot be infinitely small due to the limitation of computer capability. Thus we use a trial-and-error method to select a proper time step length which meets the requirements of both algorithm convergence and computer capability. The method is described bellow: 1) a series of time step lengths $\Delta t_1 > \Delta t_2 > \cdots > \Delta t_i > \cdots > \Delta t_{n-1} > \Delta t_n$ is given; 2) performing simulation by using each time step length and making a comparison of these results. If the results for two adjacent time step lengths (i.e. Δt_i and Δt_{i+1}) are close to each other, then Δt_i is the proper time step length for simulation.

Fig.15 shows the displacement-time curves of Node 9 simulated by central difference method with $\Delta t = 5.0\times10^{-7}$ s and $\Delta t = 2.5\times10^{-7}$ s. We can see that the two

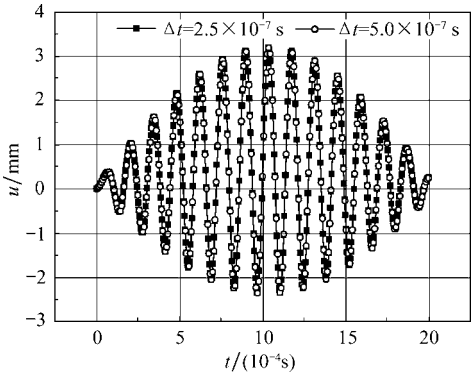

Fig.15 Convergence analysis of central difference method (frequncy of external load is 7 000 Hz).

displacement-time curves almost coincide with each other. Thus the time step length Δt=5.0×10^{-7} s is selected for central difference method. Similarly, Fig.16 shows the results predicted by Newmark method with Δt=5.0×10^{-4} s and Δt=2.5×10^{-4} s. Based on the results we can also conclude that Δt=5.0×10^{-4} s is proper to make the Newmark method be convergent in the numerical analysis.

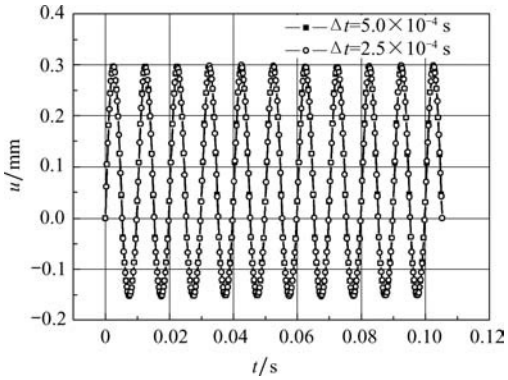

Fig.16 Convergence analysis of Newmark method (fequncy of external load is 100 Hz).

The frequency of external load is another important factor that affects the convergence of algorithm. Fig.17 shows the displacement response of Node 9 with different time step lengths predicted by central difference method. The frequency of external load is equal to 5×10^5 Hz. We can see that in the case of f=5×10^5 Hz, the algorithm cannot be convergent with Δt =5.0×10^{-7} s. A smaller time step length (such as Δt =0.5×10^{-7} s) is needed to make the algorithm be convergent.

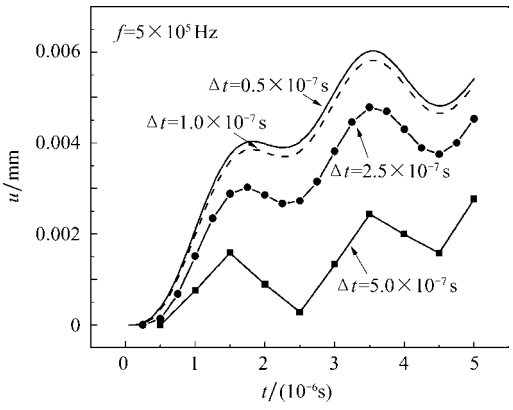

Fig.17 Displacement response of Node 9 with different time step lengths (predicted by central difference method).

Fig.18 show the displacement responses of Node 9 predicted by Newmark method. The frequencies of external load are equal to 5 Hz and 50 Hz respectively. The results show that in the case of f =5 Hz, the algorithm is convergent with Δt =0.010 s. However, when the frequency of external load rises to 50 Hz, the result with Δt =0.010 s denoted by dash line in Fig.18(b) departs from the accurate solution greatly.

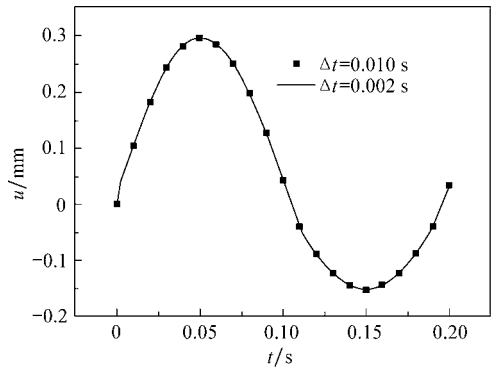

(a) Frequency of external load is 5 Hz

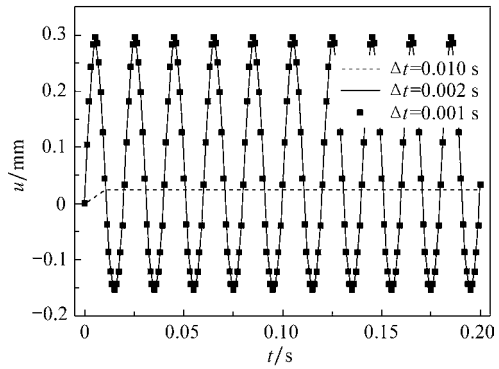

(b) Frequency of external load is 50 Hz

Fig.18 Displacement response of Node 9 with different time step lengths (predicted by Newmark method).

4.4. Effect of distributed computing system

As mentioned in Section 3.3 the distributed computing scheme can speed up the simulating process. Table 3 lists the time taken from testing processes which include 9 elements and 500 time steps for central difference method and 9 elements and 50 time steps for Newmark method respectively. By using distributed computing scheme, the stress/strain response of more than one node can be calculated parallelly with the identical time step length. Thus the entire time of testing computation is shortened. However, the speeding up ratio is not changed linearly with the increase of the number of clients strictly. For central difference method, only 42.7% (not 50%) of the time is saved by using 2 clients, and only 62.0% (not 66.7%) of the time is saved by using 3 clients. Similarly, for Newmark method, only 42.3% (not 50%) of the time is saved by using 2 clients, and only 60.9% (not 66.7%) of the time is saved by using 3 clients. This is due to the delay of signal transmission and the different computing speeds of the clients.

Table 3 Effect of distributed computing scheme on efficiency of simulation

Number of clients	Time for central difference method/min	Time for Newmark method/min
1	295	797
2	169	462
3	112	312

4.5. *Effect of matrix crack space on global dynamic response*

Matrix crack space is equal to the length of unit cell. It affects both the elastic modulus and damping capacity of CMC. Fig.19 shows the displacement response of Node 9 with different matrix crack spaces. The frequency of external load is equal to 10^5 Hz. The result indicates that decreasing the matrix crack space will increase the displacement response of the beam. This can be explained as due to the decrease of average elastic modulus when the number of matrix cracks is increased.

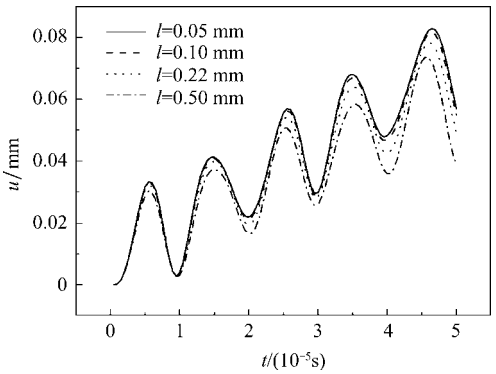

Fig.19 Effect of matrix crack space on global dynamic response (frequency of external load is 10^5 Hz, and predicted by central difference method).

5. Conclusions

In this article, a method for simulating the dynamic response of CMC beam with matrix cracks and interface debonding is proposed. Numerical results presented in the article result in the following conclusions.

(1) The stress/strain response of the unidirectional CMC with bridging matrix cracks under compressive loading exhibits nonlinear status. However, the stress-strain curve appears to be linear and the slope approaches to the elastic modulus of intact material when the compressive load increases. This can be explained as the close of matrix cracks.

(2) The displacement response of CMC beam being subjected to harmonic loading is affected by the frequency of external load greatly. If the frequency is quite low, the displacement response of CMC beam is almost periodic. In addition, the time internal between two adjacent zero-points is constant and it is equal to the period of external load. Due to the effect of interface slip, the displacement response of CMC is not symmetrical about the axis of u=0. When the frequency increases, the effect of wave on the displacement response cannot be ignored and the time internal between two adjacent zero-points is not constant. However the average period is close to the period of external load. In the case of 7 000 Hz which is close to the first order natural frequency the amplitude of displacement is quite greater than that for other frequencies. Due to the effect of damping caused by the interface friction the response of the CMC beam is limited within a finite range.

(3) Convergence and stability of the algorithm are also discussed in this article. Newmark method is unconditionally stable, but the central difference method is conditionally stable. In order to keep the central difference method be stable, the time step length Δt must be shorter than critical time step length Δt_{cr}. Since the elastic modulus of CMC varies with the changing of external load, the critical time step length of central difference method is also affected by external load. The maximum elastic modulus corresponds to the minimum critical time step length under compressive loading. Thus the minimum critical time step length which is equal to $3.230\ 7\times10^{-6}$ s is calculated by using compressive modulus (i.e. 122 GPa) and mass density (i.e. $2.578\ 5\times10^3$ kg/m^3). In order to study the effect of time step length on the convergence of the central difference method, we make a comparison between the predicted displacement-time response for Δt=5.0×10^{-7} s with that for Δt=2.5×10^{-7} s. The comparison shows that the algorithm is convergent when Δt=5.0×10^{-7} s. The similar analysis is also performed to estimate the convergence of Newmark method, and it is found that Δt=5.0×10^{-4} s is proper to make the Newmark method be convergent in this article. The frequency of external load is another important factor which should be considered to make sure that the algorithm be convergent. The test numerical examples performed in this article indicate that the time step length for assuring convergence is inversely proportional to external load frequency.

(4) Distribution computing scheme provides a feasible method to reduce the needed time of entire simulation process. For central difference method, 42.7% of the time is saved by using 2 clients, and 62.0% of the time is saved by using 3 clients. Correspondingly, for Newmark method, 42.3% of the time is saved by using 2 clients, and 60.9% of the time is saved by using 3 clients.

References

[1] Marshall D B, Evans A G. Failure mechanisms in ceramic-fiber/ceramic-matrix composites. Journal of the American Ceramic Society 1984; 68(5): 225-231.

[2] Yang J Y, Weaver J H, Zok F W. Processing of oxide composites with three-dimensional fiber architectures. Journal of the American Ceramic Society 2009; 92(5): 1087-1092.

[3] Budiansky B, Hutchinson J W, Evans A G. Matrix fracture in fiber-reinforced ceramics. Journal of Mechanics and Physics of Solids 1986; 34(2): 167-189.

[4] Walter M E, Ortiz M. Computational modeling of damage evolution in unidirectional fiber reinforced ceramic matrix composites. Computational Mechanics 1997; 20(1-2): 192-198.

[5] Lamon J. Stochastic approach to multiple cracking in composite systems based on the extreme-values theory. Composites Science and Technology 2009; 69(10): 1607-1614.

[6] Lankford J. Dynamic compressive fracture in fiber-reinforced ceramic matrix composites. Materials Science and Engineering A 1989; 107(2): 261-268.
[7] Jaminet P T, Wolfenden A, Kinra V K. Damping and dynamic elastic modulus of ceramics and ceramic-matrix composites at elevated temperatures. Baltimore: ASTM. 1992.
[8] Wang C, Zhu Z, Hou X, et al. Damping characteristics of CVI-densified carbon-carbon composites. Carbon 2000; 38(13): 1821-1824.
[9] Zhang Q, Cheng L, Wang W, et al. Effect of interphase thickness on damping behavior of 2D C/SiC composites. International Materials Week 2007; 546-549: 1531-1534.
[10] Zhang Q, Cheng L, Wang W, et al. Effect of SiC coating and heat treatment on damping behavior of C/SiC composites. Materials Science and Engineering A 2008; 473(1-2): 254-258.
[11] Liu M, Li Y, Xu F, et al. Dynamic compressive mechanical properties and a new constitutive model of 2D-C/SiC composites. Materials Science and Engineering A 2008; 489(1-2): 120-126.
[12] Cho C, Holmes J W, Barber J R. Estimation of interfacial shear in ceramic composites from frictional heating measurements. Journal of the American Ceramic Society 1991; 74(11): 2802-2808.
[13] Birman V, Byrd L W. Effect of matrix cracks on damping in unidirectional and cross-ply ceramic matrix composites. Journal of Composite Materials 2002; 36(5): 1859-1877
[14] Birman V, Byrd L W. Damping in ceramic matrix composites with matrix cracks. International Journal of Solids and Structures 2003; 40(16): 4239-4256.
[15] Birman V, Byrd L W. Matrix cracking in transverse layers of cross-ply beams subjected to bending and its effect on vibration frequencies. Composites Part B: Engineering 2001; 32(1): 47-55.
[16] Han Y M, Hahn H T. Ply cracking and property degradation of symmetric balanced laminates under general in-plane loading. Composite Science and Technology 1989; 35(4): 377-397.
[17] Beyerle D S, Spearing S M, Evans A G. Damage mechanisms and the mechanical properties of a laminated 0/90 ceramic/matrix composite. Journal of the American Ceramic Society 1992; 75(12): 3321-3330.
[18] Oden J T, Vemaganti K, Moes N. Hierarchical modeling of heterogeneous solids. Computer Methods in Applied Mechanics and Engineering 1999; 172(1-4): 3-25.
[19] Macri M, De S. An octree partition of unity method (OctPUM) with enrichments for multiscale modeling of heterogeneous media. Computers & Structures 2008; 86(7-8): 780-795.
[20] Billade N, Vemaganti K. Hierarchical models of thin elastic structures: overview and recent advances in error estimation and adaptivity. Computer Method in Applied Mechanics and Engineering 2007; 196(37-40): 3508-3523.
[21] Kwon Y W, Allen D H, Talreja R. Multiscale modeling and simulation of composite materials and structures. New York: Springer, 2007.
[22] Pant R H, Gibson R F. Analysis and testing of dynamic micromechanical behavior of composite materials at elevated temperatures. Journal of Engineering Materials and Technology 1996; 118(4): 554-560.
[23] Yang S, Gibson R F, Crosbie G M, et al. Dynamic mechanical properties of ceramics and ceramic composites at elevated temperatures. Journal of Engineering for Gas Turbines and Power 1997; 119(1): 15-19.
[24] Lee L T. A graphical compilation of damping properties of both metallic and non-metallic materials. AFML-TR-66-169, 1966.
[25] Beyerle D S, Spearing S M, Evans A G. Damage mechanisms and the mechanical properties of a laminated 0/90 ceramic/matrix composite. Journal of American Ceramic Society 1992; 75(12): 3321-3330.
[26] Erdman D L, Weitsman Y. The multi-fracture response of cross-ply ceramic composites. International Journal of Solids and Structures 1998; 35(36): 5051-5083.
[27] Delale F, Zhang H Q, Liaw B M, et al. Tensile damage behavior of ceramic matrix composites under high temperature. Fracture and Damage 1992; 27(1): 103-108.
[28] Nairn J A, Hu S. The formation and effect of outer-ply microcracks in cross-ply laminates: a variational approach. Engineering Fracture Mechanics 1992; 41(2): 203-221.
[29] Bathe K J, Wilson E L. Numerical methods in finite element analysis. New Jersey: Prentice-Hall, 1976.

Biographies:

Gao Xiguang Born in 1981, he received B.S. and Ph.D. degrees from Nanjing University of Aeronautics and Astronautics (NUAA) in 2003 and 2008 respectively, and now he is an associate professor in NUAA. His main research interest is damage mechanics of ceramic matrix composites.
E-mail: gaoxiguang@gmail.com

Song Yingdong Born in 1969, he received B.S. and Ph.D. degrees from NUAA in 1990 and 1997 respectively, and now he is a professor in NUAA. His main research interest is structure design of aeroengine.
E-mail: ydsong@nuaa.edu.cn